Facile functionalization of Fe2O3 nanoparticles to induce inherent photoluminescence and excellent photocatalytic activity

Monalisa Pal, Rupali Rakshit, and Kalyan Mandal

Citation: Applied Physics Letters **104**, 233110 (2014); doi: 10.1063/1.4882904
View online: http://dx.doi.org/10.1063/1.4882904
View Table of Contents: http://scitation.aip.org/content/aip/journal/apl/104/23?ver=pdfcov
Published by the AIP Publishing

Facile functionalization of Fe_2O_3 nanoparticles to induce inherent photoluminescence and excellent photocatalytic activity

Monalisa Pal,[a] Rupali Rakshit, and Kalyan Mandal
S.N. Bose National Center for Basic Sciences, Block-JD, Sector-3, Salt Lake, Kolkata 700098, India

(Received 18 April 2014; accepted 30 May 2014; published online 11 June 2014)

Herein, we report the emergence of intrinsic multicolor photoluminescence in Fe_2O_3 nanoparticles (NPs) ranging from blue, cyan, to green, upon facile functionalization and further surface modification with a small organic ligand, Na-tartrate. Moreover, we have found unprecedented photocatalytic property of the functionalized Fe_2O_3 NPs in the degradation of a model water-contaminant. Meticulous investigation through UV-visible absorption and fluorescence study along with theoretical support from literature unfolds that ligand-to-metal charge-transfer transition from the tartrate ligand to the lowest unoccupied energy level of Fe^{3+} of the NPs and d−d transitions centered over Fe^{3+} ions in the NPs play the key role in the emergence of multiple photoluminescence from the ligand functionalized Fe_2O_3 NPs. Moreover, vibrating sample magnetometry measurements demonstrate that the surface modification changes the magnetic behaviour of Fe_2O_3 NPs upon functionalization. We believe that the great potential of our versatile, ferromagnetic, multicolor photoluminescent Fe_2O_3 NPs would stimulate the development of numerous opportunities toward their biological and technological applications. © *2014 AIP Publishing LLC*. [http://dx.doi.org/10.1063/1.4882904]

Development of multifunctional nanoprobe combining various beneficial properties within a single entity has been a pivotal research area since the past decade. In this respect, transition metal oxide nanoparticles (NPs) have attracted utmost interest in recent years, because of their unique optical, electronic, magnetic, and catalytic properties. Moreover, nanotechnology and biology have synergized in dynamic development of a promising emerging research area called nanobiotechnology. In particular, properly functionalized magnetic NPs (MNPs) possess manifold advantages[1] which give rise to numerous exciting opportunities in the field of biomedical applications such as magnetic tweezers in magnetic separation of proteins or cells,[2] extraction of DNA molecules,[3] and therapeutic applications including AC magnetic field-assisted hyperthermia.[4] Noticeably, MNPs can be controlled by an external field, which promotes targeted delivery of radioactive isotopes and drugs for radiotherapy and chemotherapy as well as gene targeting and in noninvasive diagnosis, enhancing contrast in magnetic resonance imaging (MRI),[5] and fluorescence imaging.[6–8]

Additionally, tunable size of MNPs ranging from a few nanometers to tens of nanometers facilitates their interaction probability with different biological entities. On the other hand, MNPs have been proved to be a promising candidate in catalysis for selective chemical transformations having both economic and environmental benefits, considering their high activity, low cost, facile preparation method, adequate stability, and controlled separation by an external magnetic field.[9–13]

So far, MNPs for fluorescence imaging have been prepared either by molecular attachment with fluorescent dyes or polymers or forming nanocomposites with quantum dots (QDs).[7,8] Poor photostability of fluorescent dyes and inherent toxicity of QDs impose severe concern to their bio-imaging applications.[14] So, to solve these problems, the development of biocompatible MNPs, having intrinsic photoluminescence property and photostability, is highly desirable. Among the MNPs, Fe_2O_3 nanomaterials have attracted significant attention of the researchers because of their innate environmentally benign character and outstanding thermal stability in practical applications such as in targeted drug delivery,[15] magnetic data storage, gas sensing, Li-ion battery,[16,17] fabrication of photoanodes for photo-assisted electrolysis, pigments, and catalysis.[18–23] But the development of intrinsic photoluminescence, playing with the surface electronic structure of functionalized Fe_2O_3 NPs is sparse in literature. In spite of enormous efforts of different groups, aqueous phase insolubility and the absence of any inherent photoluminescence properties of the NPs inhibit their direct biomedical and several technological applications. Thus, fabrication of appropriately surface modified Fe_2O_3 NPs having intrinsic photoluminescence to explore its diverse biological and technological applicability is highly desirable.

Our present work reports the development of Fe_2O_3 NPs as a multifunctional nanoprobe having inherent multicolor photoluminescence, ferromagnetism, and excellent photocatalytic activity, simultaneously. Utilizing the reactivity of tartrate ligands, we have solubilized the as-prepared NPs into the water medium. Upon further surface modification of water-solubilized tartrate-functionalized Fe_2O_3 NPs, we have discovered the emergence of multicolor photoluminescence, starting from blue, cyan, to green. Mystery of the generation of this multicolor photoluminescence property can be satisfactorily solved with ligand field theory. It has been found that the ligand-to-metal charge-transfer (LMCT) from tartrate ligand to the lowest unoccupied energy levels of Fe^{3+} metal ions in the NPs and d−d transitions play the key role. Finally, we have intended to exploit the broad photo excitation (covering a large portion of UV-vis region) of the

[a]Author to whom correspondence should be addressed. Electronic addresses: monalisa.pal6@gmail.com and monalisa12@bose.res.in

functionalized Fe_2O_3 NPs in photocatalysis. Interestingly, the functionalized Fe_2O_3 NPs exhibit excellent photocatalytic property in the degradation of methylene blue (MB), a commonly used organic dye in textile industries and a model water-contaminant.

We have synthesized Fe_2O_3 NPs following a wet chemical method previously reported by Sun *et al.*, with slight modification[24] and functionalized with tartrate ligands (described in supplementary material[38] in detail). TEM (Transmission electron microscopy) study was performed to characterize the size and morphology of the as-prepared NPs shown in Fig. 1(a). TEM image of Fe_2O_3 NPs demonstrates that average size of the particles was ~50 nm. XRD (X-ray diffraction) pattern of the as-prepared NPs, shown in Fig. 1(b) exactly matches with the α phase of Fe_2O_3 (hematite, JCPDS, file no. 33-0664). The presence of a very low intensity peak corresponding to (400) plane of γ-Fe_2O_3 (maghemite, JCPDS, file no. 39-1346) in the XRD pattern of as-prepared NPs indicates that the as-prepared NPs were predominantly in α phase. EDX (Energy-dispersive X-ray) spectrum of the NPs as shown in Fig. 1(c) confirms the presence of both Fe and O. Fig. 1(d) shows the SAED (Selected area (electron) diffraction) pattern, indicating high crystallinity of the as-prepared Fe_2O_3 NPs.

To solubilize Fe_2O_3 NPs in an aqueous environment, we functionalized the as-prepared NPs with a biocompatible organic ligand, Na-tartrate. After surface functionalization, size of the highly water-solubilized NPs remained almost unchanged as evident from Fig. 1(f). The HRTEM (High-resolution transmission electron microscopy) image of tartrate-functionalized Fe_2O_3 NPs (as shown in Fig. 1(e)) clearly exhibits highly crystalline nature of the NPs. The calculated interplanar distance between the fringes has been found to be 0.28 nm corresponding to (104) plane of the α-Fe_2O_3 crystal lattice.

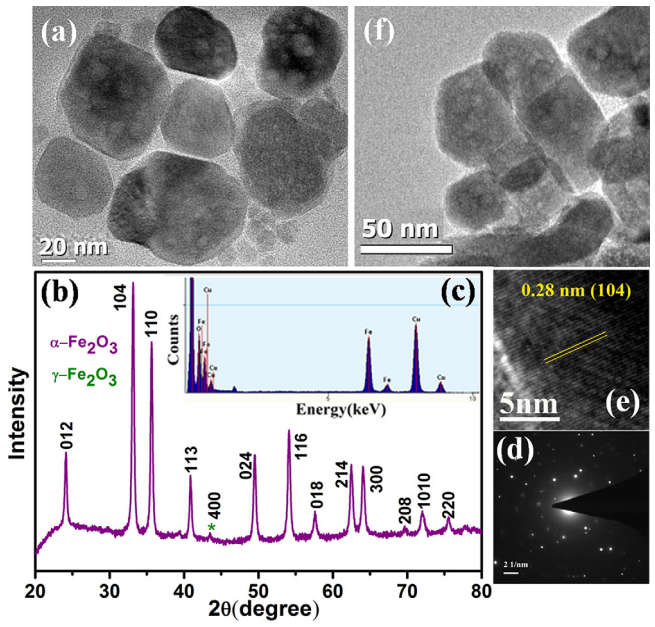

FIG. 1. (a) TEM image of the as-prepared bare Fe_2O_3 NPs. (b) XRD pattern of as-prepared Fe_2O_3 NPs. All diffraction peaks in the figure are perfectly indexed in the literature to the rhombohedral corundum structure of α-Fe_2O_3 NPs along with only one impurity peak corresponding to (400) plane of γ-Fe_2O_3. (c) EDX spectrum of the NPs indicates the presence of both Fe and O. (d) SAED pattern of as-prepared Fe_2O_3 NPs indicates high crystallinity. (e) HRTEM image of tartrate-functionalized Fe_2O_3 NPs indicates high crystallinity remains unaltered after surface modification and shows lattice fringes. (f) TEM image of the tartrate-functionalized Fe_2O_3 NPs.

FTIR (Fourier transform infrared spectroscopy) study was carried out for Fe_2O_3 NPs before and after functionalization along with the ligand alone, to confirm the attachment of ligand molecules with NPs' surface. As shown in Fig. 2(a), the characteristic peaks of Fe_2O_3 NPs at 547 and 470 cm^{-1} can be assigned to Fe-O stretching and bending vibration mode, respectively.[25] Those peaks are not distinctly visible after functionalization (i.e., in the case of the functionalized Fe_2O_3 NPs), which suggests that effective surface modification of the NPs has taken place upon interaction with tartrate ligands. Whereas, in case of tartrate, two sharp peaks arising at 1066 and 1112 cm^{-1} are due to the C–OH stretching modes,[26] and peaks at 1411 and 1621 cm^{-1} are attributed to symmetric and asymmetric stretching modes of the carboxylate groups (COO^-) of tartrate, respectively.[27] Upon interaction with the NPs' surface (i.e., in case of functionalized Fe_2O_3), all these different bands are perturbed significantly along with the band at 3399 cm^{-1}, generated due to the stretching vibrational modes of hydroxyl group (O-H),[26] clearly indicates that both $–COO^-$ and –OH groups are involved in the functionalization process.

Fig. 2(b) shows the magnetic study of both as-prepared and functionalized Fe_2O_3 NPs (inset) at room temperature. It is noteworthy that the shape of the hysteresis loop is constricted. Constricted loops are typically observed in a system having mixture of soft and hard magnetic phases. Thus, at room temperature the observed response could be due to

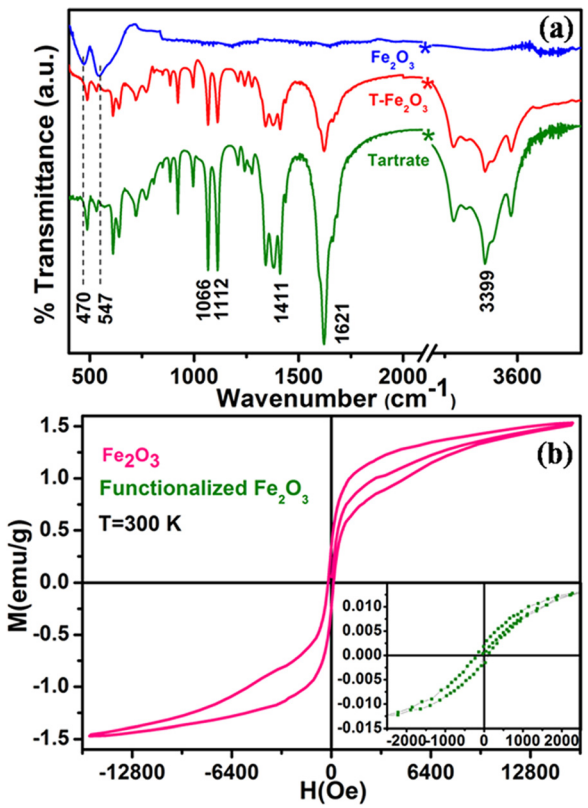

FIG. 2. (a) FTIR spectra of as-prepared Fe_2O_3 and functionalized Fe_2O_3 NPs along with Na-tartrate alone. (b) Magnetization versus applied magnetic field plot for the as-prepared bare Fe_2O_3 NPs. In the inset hysteresis loop of functionalized Fe_2O_3 NPs indicates ferromagnetic nature at room temperature (300 K).

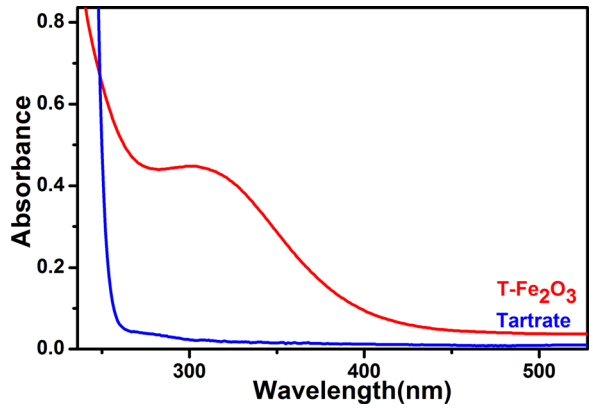

FIG. 3. UV-vis absorption spectra of functionalized Fe_2O_3 NPs and Na-tartrate.

combination of α and very small amount of γ phases (as evident from the XRD). The γ phase is a soft phase with higher moment, whereas the α phase have higher coercivity but lower moment. Combination of these two magnetic properties leads to a constricted hysteresis loop. Coercivity of as-prepared sample was found to be 174.34 Oe and the magnetization curve did not saturate up to the maximum applied magnetic field of 1.6 T. After functionalization, the magnetic behaviour of Fe_2O_3 NPs converted to typical ferromagnetic pattern with slight decrease in coercivity (145.46 Oe) and saturation magnetization. The change in magnetic behaviour upon functionalization can be explained by ligand field theory.[28] Although the oxygen coordination for Fe^{3+} ions in bulk or core Fe_2O_3, having corundum structure, is quite symmetrical in the forms of octahedron or tetrahedron, the coordination symmetry is greatly reduced for metal cations at the surface due to missing of some coordination oxygen atoms. Consequently, the magnetic structure at the surface layer could be drastically different than the core. Surface usually exhibits some degree of spin disorder and pinning. Qualitatively, adsorbed ligands can be viewed as effectively taking the positions of the missing oxygen atoms, which makes the symmetry and crystal field of the surface metal ion more closely resembling that of the core, and therefore reduces the spin disorder and pinning. Such changes certainly affect the surface anisotropy and consequently the coercivity of NPs. Tartrate ligand, containing both the σ-donor ($-OH^-$) and π-donor ($-COO^-$) functional group favours the quenching of magnetic moments of Fe^{+3} ions in the surface of functionalized Fe_2O_3 NPs, resulting a decrease in the saturation magnetization.[29] On the other hand, quenching of the magnetic moments reduces its spin-orbit coupling, leading to decrease in magnetocrystalline anisotropy, which results in reduction of coercivity[28] in functionalized Fe_2O_3 NPs as compared to the as-prepared NPs.

UV-vis absorbance spectrum of functionalized Fe_2O_3 NPs as depicted in Fig. 3 consists of a broad band having maximum at around 320 nm. Interestingly, upon exciting the sample at 320 nm, we observed photoluminescence at 410 nm, although with a low intensity. To increase the photoluminescence intensity, we performed further surface modification by heating after high pH treatment, which resulted in generation of two more photoluminescence peaks with multiple fold increase in overall intensity, upon excitation at proper wavelengths. The reason for enhancement of the photoluminescence intensity as well as generation of two more optical bands upon surface modification could be due to increased coordination between the ligand functional groups (carboxylate and hydroxyl moieties) and Fe^{3+} centers at the NP surface. Fig. 4(a) shows normalized steady-state photoluminescence emission spectra obtained from surface modified Fe_2O_3 NPs. Upon excitation at wavelengths of 320, 365, and 410 nm, the NPs solution gave rise to intense photoluminescence peaks at 410, 460, and 490 nm, respectively. Except 320 nm, other observed excitation bands at around 365 and 410 nm were not observed in the absorption spectrum (Fig. 3), presumably because these bands were masked by the more intense 320 nm absorption, however, were distinctly visible in the excitation spectrum as shown in Fig. 4(b). The photoluminescence micrographs of functionalized Fe_2O_3 NPs, demonstrate that the black powder of functionalized NPs under bright field (Fig. 4(c)), gives rise to photoluminescent colors like cyan (Fig. 4(d)) and green (Fig. 4(e)) upon excitation at 365 and 436 nm, respectively, by using

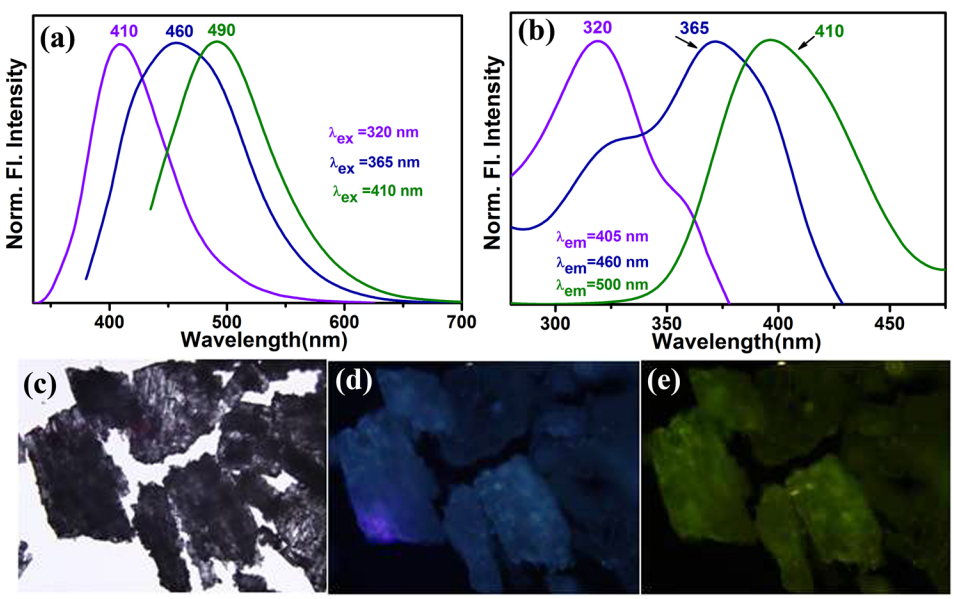

FIG. 4. (a) Normalized steady-state photoluminescence emission spectra obtained from tartrate-functionalized Fe_2O_3 NPs with three different excitation wavelengths of 320, 365, and 410 nm, respectively. (b) Photoluminescence excitation spectra of functionalized Fe_2O_3 NPs at different emission maxima of 405, 460, and 500 nm, respectively. Photoluminescence micrographs of powder functionalized Fe_2O_3 NPs under (c) bright field, (d) UV (365 nm), and (e) blue (436 nm) light irradiation.

proper filters. Noticeably, the photoluminescence microscopic images of as-prepared bare Fe_2O_3 NPs under identical conditions (as shown in Fig. S1 of the supplementary material[38]) have no such coloration. Photoluminescence quantum yields (QY) of the functionalized Fe_2O_3 NPs have been calculated by following the relative method of Williams *et al.*,[30] which involves the use of well characterized standard fluorescent compounds with known QY values. Photoluminescence QYs of 8.958% (for 410 nm band), 0.2% (for 460 nm band), and 0.5% (for 490 nm band) were obtained relative to the standard fluorescent compounds such as 2-aminopurine (2AP), 4′,6-diamidino-2-phenylindole (DAPI), and Hoechst 33258, respectively. Thus, the emergence of multicolor photoluminescence in Fe_2O_3 NPs was activated by tartrate functionalization and then reinforced by further surface modification.

The mystery of the generation of intrinsic photoluminescence can also be solved by ligand field theory.[28,31] On the basis of ligand field theory, the ligand coordination provides the crystal field splitting energy (CFSE) Δ generated from d orbitals splitting with a magnitude determined by the ligands at a given coordination symmetry. As a ligand becomes more basic, the strength of the metal-ligand σ bond increases, and consequently CFSE Δ associated with the ligand increases, which ultimately lead to the splitting between the degenerate d orbitals. On the other hand, due to the strong LMCT from HOMO (Highest occupied molecular orbital, centered in the ligand) to LUMO (Lowest unoccupied molecular orbital, centered in metal ions), bonding interaction between the metal and ligand increases significantly. Photoluminescence peak arising at 410 nm can be attributed to LMCT involving HOMO of tartrate ligand and LUMO centered over metal ion Fe^{+3}.[32] The other emission peaks at 460 and 490 nm upon excitation at 365 and 410 nm can be attributed to $^6A_{1g} \rightarrow {}^4T_{1g}$ and $^6A_{1g} \rightarrow {}^4T_{2g}$ transitions involving d-d orbitals of Fe^{3+} ions, respectively, due to the crystal field splitting of a FeO_6 octahedron with O_h symmetry as the first approximation. Both the d-d transitions are formally dipole and spin forbidden transitions, however, they can have considerable strengths due to the relaxation of selection rules by octahedral distortion and spin-orbit coupling as discussed in other Fe^{3+} ($3d^5$) containing materials.[33,34]

Considering the recent remarkable growth of nanocatalysis by engineering and manipulating various materials at the nanoscale to accelerate the rate of several beneficial reactions, we intended to utilize the strong broad excitation of the functionalized Fe_2O_3 NPs throughout the UV-vis region, in photocatalysis for waste-water treatment. Functionalized Fe_2O_3 NPs showed unprecedented photocatalytic property (as shown in Fig. 5(a)) towards the degradation of methylene blue, a commonly used dye in textile industries and a model water-contaminent, upon UV light irradiation. We have found that the photodegradation of MB in presence of functionalized Fe_2O_3 NPs takes place exponentially with time following first-order rate equation with a kinetic rate constant (k) of $27.55 \times 10^{-2}\,min^{-1}$.

We also checked the reusability of the catalyst, in every 64 min of interval. We added same dose of MB into the reaction mixture up to 10 dose, keeping the catalyst concentration fixed (without addition of extra catalyst after the 1st cycle), MB decomposition rates of different cycles were

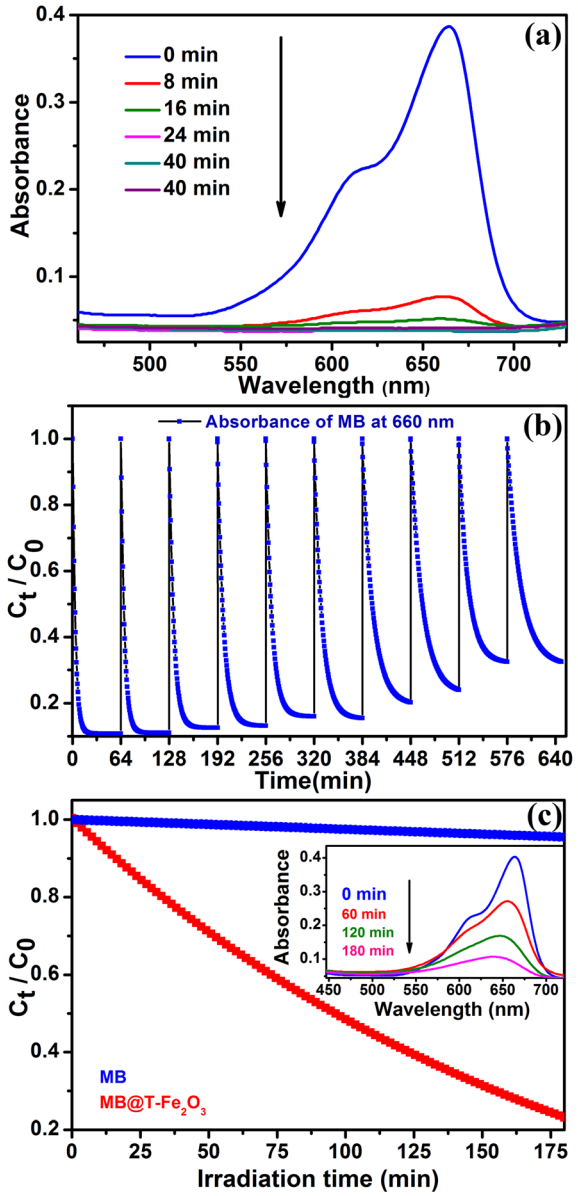

FIG. 5. (a) UV-vis spectral changes of aqueous solution of MB with time in presence of functionalized Fe_2O_3 NPs, under UV irradiation. (b) The plots of relative concentration of MB monitored at 660 nm versus time for consecutive 10 cycles, showing reusability of functionalized Fe_2O_3 NPs in MB degradation under UV light. (c) The rate of photocatalytic degradation of MB (monitored at 660 nm) in absence and presence of functionalized Fe_2O_3 NPs under visible light. Inset shows the full absorption spectra of MB in presence of functionalized Fe_2O_3 NPs with time, under visible-light irradiation.

measured by monitoring the decrease of MB absorbance at 660 nm using UV-vis spectroscopy. Fig. 5(b) shows the plots of relative concentration of MB versus time, up to 10 consecutive cycles, affirming the reusability of functionalized Fe_2O_3 NPs catalyst with almost consistent degradation rate. Having evidence from our recent findings in case of photodegradation by ligand functionalized $MnFe_2O_4$ and Mn_3O_4 NPs, we propose that the photodegradation process may follow radical pathway involving reactive oxygen species (ROS).[35–37] Furthermore, we investigated whether visible light can also activate the photocatalytic efficiency of functionalized Fe_2O_3 NPs. As shown in Fig. 5(c), we found that functionalized Fe_2O_3 NPs can degrade MB in presence of

visible light also, following 1st order reaction kinetics having rate constant (k) of $54 \times 10^{-4}\,\mathrm{min}^{-1}$. Decrease in rate of photocatalysis in presence of visible light as compared to UV light can be attributed to higher energy of UV light than visible light as well as lower absorbance of functionalized Fe_2O_3 NPs in visible region in comparison with UV region.

In conclusion, development of surface modified Fe_2O_3 NPs as multifunctional nanoprobe having simultaneously intrinsic multiple photoluminescence covering a broad range of UV-vis region from blue, cyan, to green, inherent ferromagnetism, and excellent photocatalytic properties have been achieved by a very facile ligand functionalization and subsequent surface modification strategy. Moreover, correlating with the reported theoretical aspect, we have rationally explained the emergence of the interesting optical properties. We hope that the magneto-photoluminescent Fe_2O_3 NPs will have great relevance to diverse field of biological and technological applications ranging from bioimaging, drug delivery, to nanocatalysis.

We thank CSIR for the financial grants. Authors would like to thank Mr. Mahesh Agarwal and Dr. Deepak Kumar Sinha from IACS, Kolkata for providing fluorescence microscopy facility used in this study.

[1]L. H. Reddy, J. L. Arias, J. Nicolas, and P. Couvreur, Chem. Rev. **112**(11), 5818–5878 (2012).
[2]M. Kuhara, H. Takeyama, T. Tanaka, and T. Matsunaga, Anal. Chem. **76**(21), 6207–6213 (2004).
[3]B. Yoza, A. Arakaki, K. Maruyama, H. Takeyama, and T. Matsunaga, J. Biosci. Bioeng. **95**(1), 21–26 (2003).
[4]M. Johannsen, U. Gneveckow, L. Eckelt, A. Feussner, N. Waldofner, R. Scholz, S. Deger, P. Wust, S. A. Loening, and A. Jordan, Int. J. Hyperthermia **21**(7), 637–647 (2005).
[5]H. B. Na, I. C. Song, and T. Hyeon, Adv. Mater. **21**(21), 2133–2148 (2009).
[6]J. Yang, E.-K. Lim, H. J. Lee, J. Park, S. C. Lee, K. Lee, H.-G. Yoon, J.-S. Suh, Y.-M. Huh, and S. Haam, Biomaterials **29**(16), 2548–2555 (2008).
[7]J. Gao, W. Zhang, P. Huang, B. Zhang, X. Zhang, and B. Xu, J. Am. Chem. Soc. **130**(12), 3710–3711 (2008).
[8]H. Kim, M. Achermann, L. P. Balet, J. A. Hollingsworth, and V. I. Klimov, J. Am. Chem. Soc. **127**(2), 544–546 (2005).
[9]Y. Li, H. Tan, X.-Y. Yang, B. Goris, J. Verbeeck, S. Bals, P. Colson, R. Cloots, G. Van Tendeloo, and B.-L. Su, Small **7**(4), 475–483 (2011).
[10]P. Zhang, Y. Zhan, B. Cai, C. Hao, J. Wang, C. Liu, Z. Meng, Z. Yin, and Q. Chen, Nano Res. **3**(4), 235–243 (2010).
[11]M. B. Gawande, V. D. B. Bonifacio, R. S. Varma, I. D. Nogueira, N. Bundaleski, C. A. A. Ghumman, O. M. N. D. Teodoro, and P. S. Branco, Green Chem. **15**(5), 1226–1231 (2013).
[12]M. B. Gawande, A. K. Rathi, I. D. Nogueira, R. S. Varma, and P. S. Branco, Green Chem. **15**(7), 1895–1899 (2013).
[13]M. B. Gawande, P. S. Branco, and R. S. Varma, Chem. Soc. Rev. **42**(8), 3371–3393 (2013).
[14]U. Resch-Genger, M. Grabolle, S. Cavaliere-Jaricot, R. Nitschke, and T. Nann, Nat. Methods **5**(9), 763–775 (2008).
[15]I. Milošević, S. Guillot, M. Tadić, M. Duttine, E. Duguet, K. Pierzchala, A. Sienkiewicz, L. Forró, and M.-L. Saboungi, Appl. Phys. Lett. **104**(4), 043701 (2014).
[16]C. Wu, P. Yin, X. Zhu, C. OuYang, and Y. Xie, J. Phys. Chem. B **110**(36), 17806–17812 (2006).
[17]Z. Wu, K. Yu, S. Zhang, and Y. Xie, J. Phys. Chem. C **112**(30), 11307–11313 (2008).
[18]P. Chauhan, S. Annapoorni, and S. K. Trikha, Thin Solid Films **346**(1–2), 266–268 (1999).
[19]J. S. Han, T. Bredow, D. E. Davey, A. B. Yu, and D. E. Mulcahy, Sens. Actuators, B **75**(1–2), 18–23 (2001).
[20]E. Comini, V. Guidi, C. Frigeri, I. Riccò, and G. Sberveglieri, Sens. Actuators, B **77**(1–2), 16–21 (2001).
[21]T. Ohmori, H. Takahashi, H. Mametsuka, and E. Suzuki, Phys. Chem. Chem. Phys. **2**(15), 3519–3522 (2000).
[22]W. Weiss, D. Zscherpel, and R. Schlögl, Catal. Lett. **52**(3–4), 215–220 (1998).
[23]Z. Li, P. Li, Q. Wan, F. Zhai, Z. Liu, K. Zhao, L. Wang, S. Lü, L. Zou, X. Qu, and A. A. Volinsky, J. Phys. Chem. C **117**(36), 18343–18352 (2013).
[24]S. Sun, H. Zeng, D. B. Robinson, S. Raoux, P. M. Rice, S. X. Wang, and G. Li, J. Am. Chem. Soc. **126**(1), 273–279 (2004).
[25]S. K. Sahoo, K. Agrawal, A. K. Singh, B. G. Polke, and K. C. Raha, Int. J. Eng. Sci. Technol. **2**, 218 (2010).
[26]N. Kaneko, M. Kaneko, and H. Takahashi, Spectrochim. Acta, Part A **40**(1), 33–42 (1984).
[27]V. Ramakrishnan and J. M. T. Maroor, Infrared Phys. **28**(4), 201–204 (1988).
[28]C. R. Vestal and Z. J. Zhang, J. Am. Chem. Soc. **125**(32), 9828–9833 (2003).
[29]R. Rakshit, M. Mandal, M. Pal, and K. Mandal, Appl. Phys. Lett. **104**(9), 092412 (2014).
[30]A. T. R. Williams, S. A. Winfield, and J. N. Miller, Analyst **108**(1290), 1067–1071 (1983).
[31]A. Giri, N. Goswami, M. S. Bootharaju, P. L. Xavier, R. John, N. T. K. Thanh, T. Pradeep, B. Ghosh, A. K. Raychaudhuri, and S. K. Pal, J. Phys. Chem. C **116**(48), 25623–25629 (2012).
[32]I. P. Pozdnyakov, A. V. Kolomeets, V. F. Plyusnin, A. A. Melnikov, V. O. Kompanets, S. V. Chekalin, N. Tkachenko, and H. Lemmetyinen, Chem. Phys. Lett. **530**(0), 45–48 (2012).
[33]X. S. Xu, T. V. Brinzari, S. Lee, Y. H. Chu, L. W. Martin, A. Kumar, S. McGill, R. C. Rai, R. Ramesh, V. Gopalan, S. W. Cheong, and J. L. Musfeldt, Phys. Rev. B **79**(13), 134425 (2009).
[34]J. H. Jung, M. Matsubara, T. Arima, J. P. He, Y. Kaneko, and Y. Tokura, Phys. Rev. Lett. **93**(3), 037403 (2004).
[35]M. Pal, R. Rakshit, and K. Mandal, ACS Appl. Mater. Interfaces **6**(7), 4903–4910 (2014).
[36]A. Giri, N. Goswami, M. Pal, M. T. Zar Myint, S. Al-Harthi, A. Singha, B. Ghosh, J. Dutta, and S. K. Pal, J. Mater. Chem. C **1**(9), 1885–1895 (2013).
[37]A. Giri, N. Goswami, C. Sasmal, N. Polley, D. Majumdar, S. Sarkar, S. N. Bandyopadhyay, A. Singha, and S. K. Pal, RSC Adv. **4**(10), 5075–5079 (2014).
[38]See supplementary material at http://dx.doi.org/10.1063/1.4882904 for Fluorescence micrographs of as-prepared Fe_2O_3 NPs and experimental section.